Impedance spectroscopy models for the complete characterization of thermoelectric materials

Jorge García-Cañadas and Gao Min

Articles you may be interested in

Improved thermoelectric properties of PbTe0.5Se0.5
AIP Conf. Proc. **1447**, 1027 (2012); 10.1063/1.4710356

Spectroscopy of electronic thermal noise as a direct probe of absolute thermoelectric coefficients
J. Appl. Phys. **109**, 073701 (2011); 10.1063/1.3553642

Thermoelectric characterization by transient Harman method under nonideal contact and boundary conditions
Rev. Sci. Instrum. **81**, 044902 (2010); 10.1063/1.3374120

Physical properties of Hastelloy® C-276™ at cryogenic temperatures
J. Appl. Phys. **103**, 064908 (2008); 10.1063/1.2899058

Thermoelectric cooling at cryogenic temperatures
Appl. Phys. Lett. **83**, 2142 (2003); 10.1063/1.1610810

Impedance spectroscopy models for the complete characterization of thermoelectric materials

Jorge García-Cañadas[a)] and Gao Min
School of Engineering, Cardiff University, Cardiff CF24 3AA, United Kingdom

This paper analyses the use of impedance spectroscopy as a characterization tool applied to thermoelectric materials. The impedance function of the thermoelectric system under adiabatic conditions and Peltier mode operation is calculated by solving the heat equation in the frequency domain. The analysis, focused on the complex plane, provides the required equivalent circuit elements to interpret the impedance measurements. Using this approach, all the relevant thermoelectric parameters and thermal properties can be potentially extracted at a given temperature from the impedance spectra, i.e., the Seebeck coefficient, electrical resistivity, thermal conductivity, figure of merit (zT), specific heat, and thermal diffusivity. This can be done without the need of measuring temperature differences. To validate the models described, impedance measurements have been carried out in single thermoelectric elements and modules, showing an excellent agreement with the theory. The simple nature of the measurements in conjunction with the advantage of obtaining all the important thermoelectric parameters opens up the possibility of establishing impedance spectroscopy as a very useful characterization method for the thermoelectric field. © 2014 AIP Publishing LLC. [http://dx.doi.org/10.1063/1.4901213]

I. INTRODUCTION

Electrical impedance spectroscopy (IS) is a characterization technique widely used in several fields of research (photovoltaics,[1,2] fuel cells,[3] supercapacitors,[4] corrosion,[5] etc.). The main advantage of this method over other characterization tools resides in the ability to separate the electronic related processes occurring in the device. This is achieved by measuring the impedance response of the system when a small amplitude ac signal (either voltage or current) oscillates around a certain steady state value. The response is monitored as a function of frequency and hence, rapid processes show up at high frequencies, while slow processes only appear at low frequencies.

The characterization of thermoelectric (TE) materials requires determining the variation with temperature of 3 parameters: Seebeck coefficient (S), electrical conductivity (σ), and thermal conductivity (λ). In addition, the figure of merit z, which is given by the combination of the previous parameters ($z = S^2\sigma/\lambda$), is usually given as information about the efficiency of the material. Currently, despite of the extended number of homemade techniques that exist in the literature,[6,7] there is not a widely used standard apparatus able to measure all the TE properties. On the other hand, frequently the characterization of the materials involves the use of up to 3 different pieces of equipment. Especially, the thermal conductivity is difficult to measure and requires very expensive apparatus. Under this scenario, it is worthwhile looking at developing new methods and characterization techniques. Due to the successful application of IS in other fields, it stands as a reliable technique,

and powerful apparatus are available from different manufactures in the market, so it appears interesting to explore its application in the TE area.

On this respect, some efforts have been made in the past mainly from two research groups. Hogan *et al.* first reported IS measurements of TE elements and modules and proposed the use of RC one-port and thermal transmission line models to analyze the impedance results.[8] On the other hand, De Marchi *et al.* have published several articles[9,10] analyzing the heat balance equation in the context of thermal impedance to improve the accuracy in the determination of zT (where T is the absolute temperature). However, although the possibility of using the IS technique to extract all TE properties have been pointed out by both groups, the detailed approaches and experimental verification have not been explored. To date, the attention has mostly focused on obtaining the figure of merit. A search through recent literature only turned up two papers using IS to evaluate the figure of merit.[11,12]

In this work, we focus on the development of suitable equivalent circuit elements for the interpretation of impedance results and on exploiting the capability of this method to provide a complete characterization of TE elements. We first describe the electrical impedance models required to correctly interpret the experimental results by solving the heat equation in the frequency domain under adiabatic conditions and Peltier mode operation. Then, experimental data of TE materials are analyzed employing a fitting routine to the theoretical models. All the TE parameters (the Seebeck coefficient, electrical resistivity, and thermal conductivity) and thermal properties (specific heat and thermal diffusivity) can be obtained; proving the suitability of the models and the potential of IS as a very useful characterization method for TEs.

[a)]Author to whom correspondence should be addressed. Electronic mail: jorge.garcia.canadas@gmail.com.

116, 174510-1

II. IMPEDANCE MODELS

The impedance $Z = V/I$ of a TE element with a certain cross-sectional area A and length L contacted by two metallic contacts of length L_M (Fig. 1) is given by the ratio of the potential difference V across the element to the current I flowing through the external circuit. Under operation, the voltage drop of the system presents two contributions, the one due to the ohmic resistance R of the system (which includes the intrinsic electric resistances of the material R_i and metallic contacts R_m, and the contact resistances R_c) and the one produced by the Seebeck effect. Taking this into account, the impedance function becomes

$$Z = R + \frac{S[T(L) - T(0)]}{I}, \tag{1}$$

where $T(0)$ and $T(L)$ are the temperatures at $x = 0$ and $x = L$, respectively. Our analysis neglects the Seebeck effect in the contacts since metals usually present much smaller S than TE materials and is restricted to impedance measurements performed under a small ac perturbation around an initial steady state of thermal equilibrium. In this way, the temperature difference is expected to be very small and it is assumed that all the TE coefficients and thermal properties are independent of temperature.

It is clear from Eq. (1) that to identify the impedance function, it is necessary to know the evolution with frequency of the temperatures at the edges of the TE element $T(L)$-$T(0)$. This involves solving the heat equation of the system. For this purpose, adiabatic conditions were considered and the Joule effect was neglected[9] due to the low electrical resistivity of the materials and the small currents involved. Under these assumptions (adiabatic boundaries and thermal properties independent of T), the temperature at $L_H = L/2$ remains always constant, i.e., the heat flowing in from the left equals the one flowing out to the right,

resulting $T(L_H) = T_i$ at any given time t (see Fig. 1). De Marchi et al.[10] solved this equation under these conditions in the framework of thermal impedance. The analysis is extended here for the electrical impedance and with a more detailed focus on the resulting equivalent circuit elements and the response in the complex plane plots. This will be performed with and without the influence of metallic contacts.

A. No contact influence

In a first approach, the presence of the contacts was neglected (extremely thin contacts assumption). It should be noted that in reality contacts are always needed, otherwise no Peltier effect will be produced. The heat equation of the system shown in Fig. 1 is given by

$$\frac{\partial^2 T}{\partial x^2} = \frac{1}{\alpha_{TE}} \frac{\partial T}{\partial t}, \quad \text{at } 0 < x < L, \tag{2}$$

where α_{TE} is the thermal diffusivity of the TE element, which is related to the thermal conductivity (λ_{TE}), the mass density (ρ_{TE}), and the specific heat (C_{pTE}) of the TE element by $\alpha_{TE} = \lambda_{TE}/\rho_{TE}C_{pTE}$. If $\Delta T = (T - T_i)$ is considered as the temperature difference respect to T_i, then $\partial(\Delta T) = \partial T$. Using this equivalence and the Laplace transform[13,14]

$$L[\Delta T] = \int_0^\infty \Delta T \exp(-j\omega t)dt = \theta. \tag{3}$$

Equation (2) was converted from the time domain into the frequency domain ($j\omega$)

$$\frac{\partial^2 \theta}{\partial x^2} - \frac{j\omega}{\alpha_{TE}}\theta = 0 \quad \text{at } 0 < x < L, \tag{4}$$

where $j = \sqrt{-1}$ is the imaginary number and ω is the angular frequency, defined by $\omega = 2\pi f$, with f the oscillating frequency of the ac signal.

The solution and derivative $\partial\theta/\partial x$ of Eq. (4) are given by

$$\theta(x, j\omega) = C_1 \sinh\left[\frac{x}{L_H}\left(\frac{j\omega}{\omega_{TE}}\right)^{0.5}\right]$$
$$+ C_2 \cosh\left[\frac{x}{L_H}\left(\frac{j\omega}{\omega_{TE}}\right)^{0.5}\right]^{0.5}, \tag{5}$$

$$\frac{\partial\theta}{\partial x}(x, j\omega) = \frac{1}{L_H}\left(\frac{j\omega}{\omega_{TE}}\right)^{0.5}\left\{C_1\cosh\left[\frac{x}{L_H}\left(\frac{j\omega}{\omega_{TE}}\right)^{0.5}\right]\right.$$
$$\left. + C_2\sinh\left[\frac{x}{L_H}\left(\frac{j\omega}{\omega_{TE}}\right)^{0.5}\right]\right\}, \tag{6}$$

where C_1 and C_2 are constants and ω_{TE} is the characteristic angular frequency, which is related to the thermal diffusivity and length by

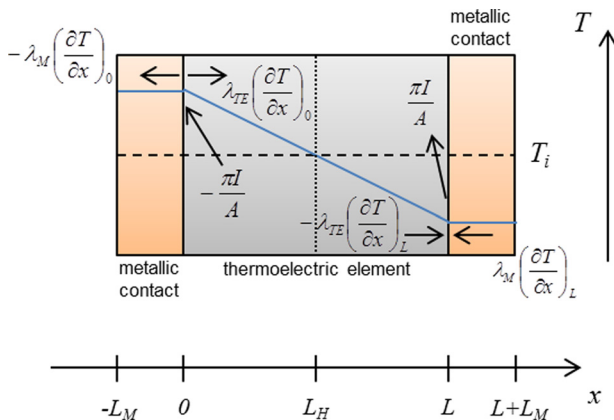$$\omega_{TE} = \frac{\alpha_{TE}}{L_H^2}. \tag{7}$$

FIG. 1. Physical model of a thermoelectric element contacted by two metallic contacts. The arrows indicate the direction of the conducting heat fluxes appearing at the junctions as a consequence of the Peltier effect when an *n*-type TE material and a positive current are considered. For the Peltier heat, the arrows point to the junction when electrons dissipate heat to the lattice and out of the junction when the electrons absorb heat from the lattice. The solid line depicts qualitatively the thermal profile at steady state. The dotted line shows the plane where the temperature remains constant at any time. The dashed line indicates the initial temperature.

The boundary conditions given by the constant temperature plane ($x = L_H$) and the adiabatic boundaries can be also defined in the frequency domain as

$$\theta(L_H) = 0, \quad \text{at } x = L_H, \qquad (8.1)$$

$$-\frac{\pi_0 i_0}{A} + \lambda_{TE}\left(\frac{\partial\theta}{\partial x}\right)_0 = 0, \quad \text{at } x = 0, \qquad (8.2)$$

where π_0 and i_0 are the Peltier coefficient and the Laplace transform of the current $(L[I] = i)$ at $x = 0$. Applying these boundary conditions to Eqs. (5) and (6), the integration constants can be obtained

$$C_1 = \frac{\pi_0 i_0 L_H}{\lambda_{TE} A}\left(\frac{j\omega}{\omega_{TE}}\right)^{-0.5}, \qquad (9)$$

$$C_2 = -\frac{\pi_0 i_0 L_H}{\lambda_{TE} A}\left(\frac{j\omega}{\omega_{TE}}\right)^{-0.5}\tanh\left\{\left(\frac{j\omega}{\omega_{TE}}\right)^{0.5}\right\}. \qquad (10)$$

$T(L)$-$T(0)$, which is needed for the calculation of the impedance (Eq. (1)), is given in the frequency domain by $-2\theta(0)$. Using this and the Kelvin relationship $\pi_0 = ST(0)$, the impedance function in the frequency domain can be obtained

$$Z(j\omega) = R + \frac{S^2 T_i L}{\lambda_{TE} A}\left(\frac{j\omega}{\omega_{TE}}\right)^{-0.5}\tanh\left\{\left(\frac{j\omega}{\omega_{TE}}\right)^{0.5}\right\}, \qquad (11)$$

taking into account that $T(0) \approx T_i$ (due to the small ac signal applied). It can be observed that a TE resistance $R_{TE} = S^2 T_i L / \lambda_{TE} A$ appears in the equation. This resistance accounts for the losses due to the existence of the Seebeck voltage V_S and was defined previously as $R_{TE} = V_S/I$.[15] It is interesting to note that the last term of Eq. (11) takes the form of a constant-temperature Warburg (W_{CT})

$$Z_{WCT}(j\omega) = R_{TE}\left(\frac{j\omega}{\omega_{TE}}\right)^{-0.5}\tanh\left\{\left(\frac{j\omega}{\omega_{TE}}\right)^{0.5}\right\}. \qquad (12)$$

We use this denomination due to the similarity with a finite-length Warburg with transmissive boundary (short Warburg) element frequently used in electrochemistry,[16] which relates to the Poisson-Nernst-Planck model.[17] It should be noted that although the equations are the same, the physical meaning of the parameters completely differs.

Fig. 2(a) shows the impedance response and its corresponding equivalent circuit of Eq. (11) using typical values corresponding to a Bi_2Te_3 TE element. Two regions appear in the figure, which are separated by a turnover frequency $\omega \approx 2pi\omega_{TE}$ ($pi = 3.14$). At this angular frequency, the magnitude of the impedance is $R_{TE}/3$. At high angular frequencies $\omega \gg 2pi\omega_{TE}$, if the influence of R is discarded ($R = 0$), Eq. (11) becomes

$$Z = \frac{S^2 T_i L}{\lambda_{TE} A}\left(\frac{j\omega}{\omega_{TE}}\right)^{-0.5} = \frac{2S^2 T_i}{A\sqrt{\lambda_{TE}\rho_{TE}C_{pTE}}}(j\omega)^{-0.5}. \qquad (13)$$

Due to the proportionality $Z(j\omega) \propto (j\omega)^{-0.5}$, a 45° line (slope 1) is expected as shown clearly in Fig. 2(a). At low angular

frequencies $\omega \ll 2pi\omega_{TE}$, the reciprocal of the impedance (admittance) is given (when $R = 0$) by

$$Z^{-1} = \frac{1}{R_{TE}} + \frac{1}{3}\frac{j\omega}{R_{TE}\omega_{TE}}, \qquad (14)$$

which corresponds to the response of a semicircle (Fig. 2(a)).

A previously reported[15] TE capacitance can be obtained from $C_{TE} = 1/R_{TE}\omega_{TE}$. This capacitance, which controls the imaginary response of the admittance at low frequencies, is determined by the thermal process, which induces the Seebeck voltage $C_{TE} = Idt/dV_S$. It can be seen that at steady state ($\omega \rightarrow 0$), the impedance defined by Eq. (11) becomes $Z = R_{TE}$, and hence, the distance between the real axis intercepts directly provide R_{TE} (Fig. 2(a)). The total impedance of the system at steady state or dc resistance is given by $R_{dc} = R + R_{TE}$.

B. Contact influence

In order to evaluate the influence of the metallic contacts, it is needed to solve the heat equation considering their influence. Following the same procedure as above, it can be obtained in the frequency domain

$$\frac{\partial^2\theta}{\partial x^2} - \frac{j\omega}{\alpha_M}\theta = 0, \quad \text{at } -L_M < x < 0, \qquad (15)$$

where α_M is the thermal diffusivity of the metal, which is related to the thermal conductivity (λ_M), the mass density (ρ_M), and specific heat (C_{pM}) of the contact by $\alpha_M = \lambda_M/\rho_M C_{pM}$. The boundary conditions are given by

$$\left(\frac{\partial\theta}{\partial x}\right)_{-L_M} = 0, \quad \text{at } x = -L_M, \qquad (16.1)$$

$$-\frac{\pi_0 i_0}{A} - \lambda_M\left(\frac{\partial\theta}{\partial x}\right)_{0,M} + \lambda_{TE}\left(\frac{\partial\theta}{\partial x}\right)_{0,TE} = 0, \quad \text{at } x = 0, \qquad (16.2)$$

$$\theta(0)_M = \theta(0)_{TE}, \quad \text{at } x = 0. \qquad (16.3)$$

Equation (16.3) ensures the temperature continuity at $x = 0$. After solving the system of equations (Eqs. (4), (8.1), (8.2), (15), and (16.1)–(16.3)) and introducing the resulting expression for $\theta(0)$ in the impedance function, it can be found that

$$Z = R + \left(\frac{1}{Z_{WCT}^{-1} + Z_{Wa}^{-1}}\right), \qquad (17)$$

where

$$Z_{Wa} = R_M\left(\frac{j\omega}{\omega_M}\right)^{-0.5}\coth\left\{\left(\frac{j\omega}{\omega_M}\right)^{0.5}\right\}, \qquad (18)$$

is defined as an adiabatic Warburg (W_a), which shows a similar expression to a finite-length Warburg with blocking boundary element (open Warburg) from the Poisson-Nernst-Planck model.[16,17] In Eq. (18), $\omega_M = \alpha_M/L_M^2$ is the characteristic angular frequency of thermal diffusion in the metallic
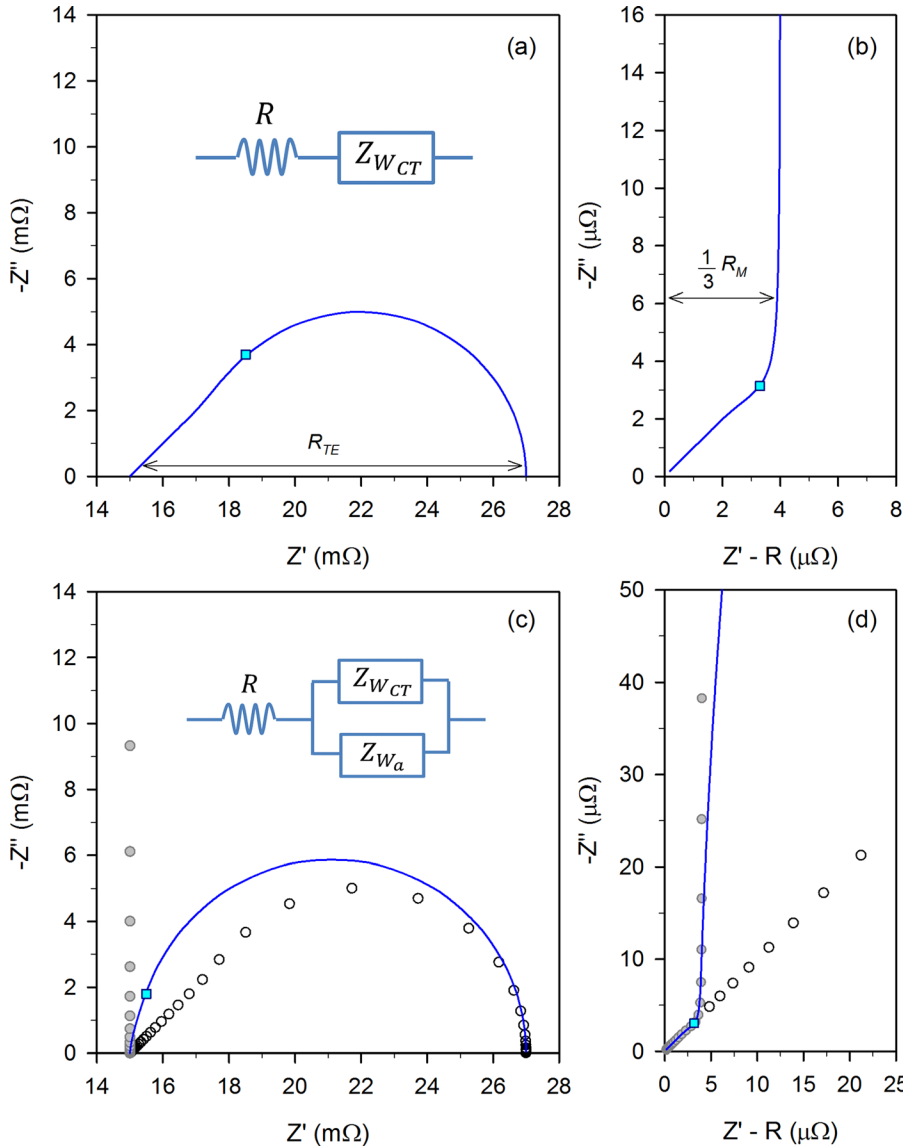
FIG. 2. Simulated impedances for a Bi$_2$Te$_3$ thermoelectric element with $A = 1$ mm^2, $L = 1.5$ mm, $\alpha_{TE} = 0.011$ cm^2/s, $\lambda_{TE} = 1.5$ W/mK, at $T_i = 300$ K. The square indicates the characteristic angular frequencies ω_c that separates the Nyquist plot into linear and semicircle regions. (a) Under no contact influence using the equivalent circuit in the inset, the characteristic frequency is $\omega_c = 2pi\omega_{TE} = 12.6$ rad/s. (b) Under contact influence and assuming that the Peltier flux is only conducted towards the metallic contact. Using $L_M = 0.2$ mm, $\alpha_M = 1.11$ cm^2/s, $\lambda_M = 400$ W/mK, and $\omega_c = 2pi\omega_M = 17436$ rad/s. The value of the series resistance R has been subtracted in the real axis to gain clarity. (c) With contact influence using the equivalent circuit of the inset, with $\omega_c = 2pi\omega_{TE} = 12.6$ rad/s (solid line). The empty circles represent the same plot of (a) and the solid circles represent the same plot of (b) with the presence of R. (d) The blow-up at high frequency region in plot, (c) where R has also been subtracted in the real axis and the solid square represents the characteristic frequency $\omega_c = 2pi\omega_M$ due to metal contact.

contact and $R_M = 2S^2 T_i L_M / \lambda_M A$ is a TE resistance related to energy loss in the metal contact due to the existence of the Seebeck voltage in the system. It can be seen from Eq. (17) that the total impedance of the system consists of a pure resistance R connected in series with two parallel connected Warburg elements (Z_{WCT} and Z_{Wa}). The corresponding equivalent circuit is shown by the inset of Fig. 2(c). It can be observed that when $L_M \rightarrow 0$ (no contact influence approximation), Eq. (17) equals Eq. (11).

The response of the adiabatic Warburg results from heat diffusion taking place from $x = 0$ towards $x = -L_M$. Assuming that the Peltier heat is only conducted into the metal contacts, the impedance of the system (discarding R) can be calculated using Eq. (18). Fig. 2(b) shows the result obtained using typical thermal properties of Cu. The characteristic angular frequency $\omega = 2pi\omega_M$ separates the Nyquist plot into two regions. At $\omega \gg 2pi\omega_M$, Eq. (18) becomes

$$Z = R_M \left(\frac{j\omega}{\omega_M} \right)^{-0.5} = \frac{2S^2 T_i}{A \sqrt{\lambda_M \rho_M C_{pM}}} (j\omega)^{-0.5}. \quad (19)$$

At low frequencies ($\omega \ll 2pi\omega_M$), the impedance is given by

$$Z = \frac{1}{3} R_M + \frac{R_M \omega_M}{j\omega}. \quad (20)$$

It can be seen that the real part of the impedance is a constant, $R_M/3$ (Fig. 2(b)). At these frequencies, the temperature change in the contact is mainly governed by the specific heat (accumulation of heat). This can be seen from the second term in Eq. (20), which becomes larger at lower frequencies and only contains C_{pM} as thermal parameter. It should be noted that from the value of R_M, it is possible to obtain the S of the TE material since the thermal conductivity of the metallic contact (typically Cu or Ni) is usually known. We exploit this below to provide a complete characterization of all the TE parameters.

Fig. 2(c) shows the total impedance of the system calculated using Eq. (17) based on a Cu/Bi$_2$Te$_3$ system. Fig. 2(d) displays the blow-up of the high frequency region of Fig. 2(c). It can be seen that in this regime, the response is dominated by the properties of contacts. When $\lambda_M \gg \lambda_{TE}$, the TE material behaves nearly as a thermal insulator. However, if the thermal conductivities of the contacts and TE material do not differ greatly, a contribution from both metal and TE element
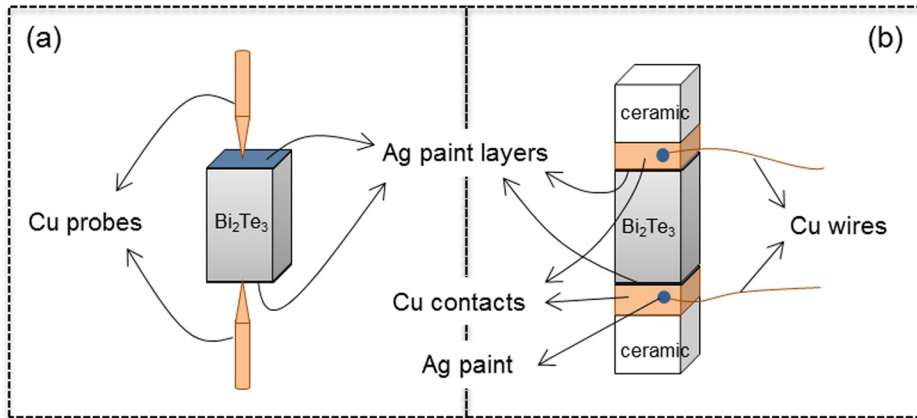
FIG. 3. Sketch of the thermoelements prepared for the impedance measurements. (a) Sample with very thin Ag paint contacts contacted by sharpened Cu probes. (b) Sample with Cu/ceramic contacts contacted by thin Cu wires.

is expected. At low frequencies, the Nyquist plot becomes almost a perfect semicircle (Fig. 2(c)), indicating that the thermal process in this regime is dominated by the response of the TE element (Eq. (11)). The total impedance of the system at steady state (i.e., $\omega = 0$) becomes a pure resistance with a value given by $R_{dc} = R + R_{TE}$, as if no contact exists.

III. EXPERIMENTAL VALIDATION

In order to experimentally validate the developed theoretical models, the impedance response of p-type Bi_2Te_3 elements (European Thermodynamics Ltd.) with a cross-sectional area of $1.4 \times 1.4 \, mm^2$ and a length of 1.6 mm were measured. The first sample was designed to have very thin contacts and was prepared by spreading a layer of Ag paint on the top and bottom sides of the element (Fig. 3(a)). This sample was sandwiched by two short Cu probes with sharp tips that were connected to the input leads of the equipment. The length of the leads was minimized as much as possible to avoid a significant contribution from their inductance in the measurements. The tips were sharpened to minimize the heat conduction through these probes. A second sample was prepared with thick contacts that consist of two-layer structure of Cu/ceramic contacts as typically used in TE modules (Fig. 3(b)). The Cu/ceramic pieces have the same cross-sectional area as that of the TE element and the thickness of 0.4 mm and 0.8 mm, respectively. The contacts were attached to the TE element using Ag paint. Finally, very thin Cu wires were attached to the Cu contacts using Ag paint. In addition, a commercial TE module (European Thermodynamics Ltd.) formed

by 254 thermoelements ($1 \, mm \times 1 \, mm \times 1.5 \, mm$) was also investigated, which was suspended in air during measurements to provide adiabatic conditions. The thickness of ceramic plates of the module is 0.8 mm.

Impedance measurements were performed on the thermoelements at room temperature using a PGSTAT302N potentiostat equipped with a FRA32M impedance module (Metrohm Autolab B. V.) in a frequency range of 10 mHz to 100 Hz. An inductive-like response was observed at frequencies higher than 100 Hz but this was discarded from our analysis. A sinusoidal signal of 20 mA (rms) in amplitude was applied without dc bias (0 A dc). The 20 mA rms amplitude corresponds to ≈ 1.75 mV rms for the sample with very thin contacts (Fig. 3(a)). When the elements were measured, the first results were discarded since shifts to lower values in the real part of the impedance were observed, probably due to the change of the contact properties when current flows through for the first time. Alternatively, a current can be applied to the sample for a few seconds before running the impedance. For the TE module, impedance measurements were performed in a frequency range of 1 mHz to 1 kHz with an ac voltage of 10 mV (peak) in amplitude and without dc bias. This frequency range was also selected to exclude the high-frequency inductive response. All the measurements performed showed good repeatability (around 2% deviation). Fitting of experimental data to the appropriate equivalent circuits was performed using Zview 3.3 software.

Fig. 4 shows the experimental results of the TE elements described in Fig. 3. Since the size of the samples and the temperature variations across the thermoelements are small,
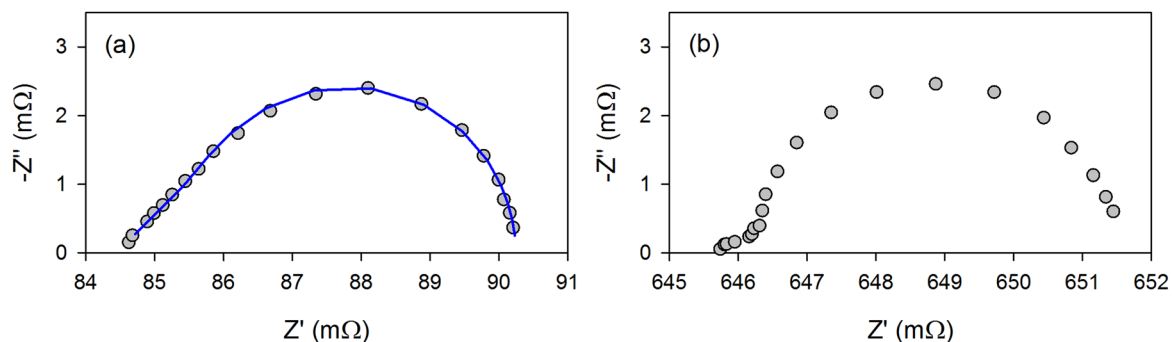

FIG. 4. Impedances of p-type thermoelements with very thin Ag contacts (a) and with Cu/ceramic contacts (b). Line in (a) represents the fitting to the equivalent circuit in Fig. 2(a).

TABLE I. Fitting parameters and extracted thermal properties.

Sample	R (Ω)	R_{TE} (Ω)	ω_{TE} (rad/s)	C_{TE} (F)	λ_{TE} (W/mK)	α_{TE} (cm²/s)	C_{pTE} (J/gK)	S (μV/K)	R_c (Ω)	ω_c (rad/s)
Element	0.084	0.0058	2.0	86.21	1.27	0.013	0.13	…	…	…
Module	4.292	2.585	0.24	1.61	1.60	0.0013	1.56	191.5	0.149	6.08

the heat loss due to convection is negligible and hence the system is close to adiabatic conditions. The response in Fig. 4(a) corresponds to the TE element with thin Ag paint contacts (Fig. 3(a)). Clearly, it exhibits a similar shape to Fig. 2(a). By fitting the results to the equivalent circuit considering no contact influence (inset of Fig. 2(a)), the values for R, R_{TE}, and ω_{TE} can be extracted (see Table I). An excellent fitting was achieved with less than 2% errors. It is to be noted that R determined from this experiment consists of the resistances of the TE element, contacts, and wires. In order to determine the resistivity of the TE element (without influence of contact and wire), additional two probes are needed (4-probe method).

The thermal diffusivity of the TE material can be calculated directly from ω_{TE} (Eq. (7)). Using the S value obtained from a hot probe apparatus (175 μV/K), the thermal conductivity can be determined from R_{TE} and the specific heat from C_{TE} ($T_i = 300$ K and $\rho_{TE} = 7.7$ g/cm³ values were used). All these values are summarized in Table I and show similar values to typical Bi$_2$Te$_3$ samples,[18] demonstrating the feasibility of determining thermoelectric properties using the proposed impedance technique. It should be noted that a major advantage of this approach is its ability to determine several thermal parameters (thermal diffusivity, thermal conductivity, and specific heat) from a relatively simple impedance measurement.
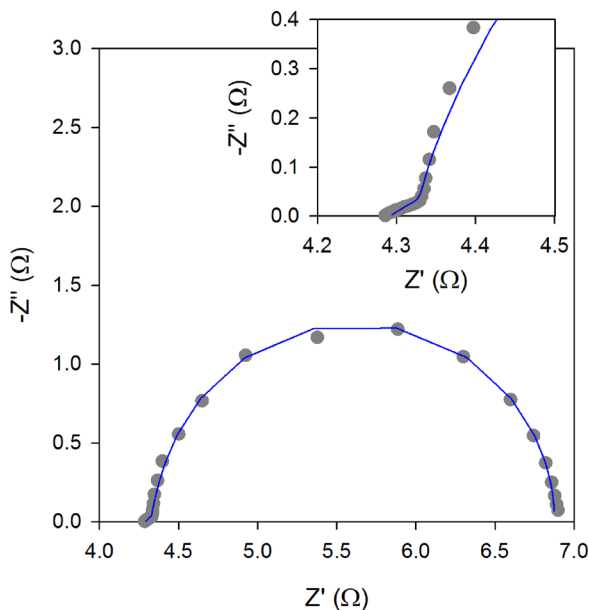

FIG. 5. Nyquist plot of a 254-leg thermoelectric module measured at "adiabatic" condition with the module suspended in air. The inset shows a magnified high-frequency part. The line corresponds to the fitting to a pure resistance (R) connected in series with parallel connected constant-temperature Warburg element (Z_{WCT}) and adiabatic Warburg element (Z_{Wa}). The fitting provides R = 4.29 Ω, R$_c$ = 0.149 Ω, ω_c = 6.08 rad/s, R$_{TE}$ = 2.585 Ω, and ω_{TE} = 0.24 rad/s.

The impedance response of the TE element with Cu/ceramic contacts (Fig. 3(b)) is shown in Fig. 4(b). It can be seen that the Nyquist plot in this case shows a semicircle with a linear part (45° slope) significantly shortened. This result is in good agreement with that predicted by the equivalent circuit considering the contact influence (Fig. 2(c)). Due to the high sensibility required for impedance measurement at these high frequencies (45° slope zone), the accuracy of the measurements were affected by the noises and it was not possible to obtain a good fit from Fig. 4(b). However, we believe that the accuracy of measurements can be improved by using a thicker ceramic or a contact material with lower thermal conductivity such as stainless steel.

As an alternative to this, an experiment was carried out using a TE module to demonstrate the possibility of providing a complete TE characterization using the impedance method. Fig. 5 shows the impedance results of the module investigated. It shows the same shape as in Fig. 4(b) (Eq. (17)) and a good fit was obtained. Due to small thickness and high thermal conductivity ($\lambda_{Cu} \approx 400$ W/mK) of the Cu layer, its influence in the spectrum can be neglected and the ceramic layer becomes the only dominant factor that determines the impedance response at these high frequencies. Neglecting the spreading-constriction thermal process[19] in the ceramic layer and using the thermal conductivity of 30 W/mK (for aluminum oxide ceramic), the S of the TE material can be calculated from $R_C/254 = 2S^2T_iL_C/\lambda_C A$, which gives 191.5 μV/K. Note that C is used now as the subscript to account for the ceramic instead of the metal (M). Once S is determined, the rest of the TE properties can be easily calculated (see Table I). In this way, a value for $\lambda_{TE} = 1.60$ W/mK was found from $R_{TE}/254 = S^2T_iL/\lambda_{TE}A$, which are very close to the typical values for Bi$_2$Te$_3$. It should be noted that the values of α_{TE} and C_{pTE} deviate around an order of magnitude respect to the typical Bi$_2$Te$_3$ values in this case. This is due to the fact that ω_{TE} is now influenced by the contact and it is not only determined by the diffusion of heat in the TE material. Diffusion also occurs in the contact, which makes the effective thermal diffusivity smaller (lower heat diffusion rate). The calculated $R = 4.29$ Ω gives the contribution of both TE element and parasitic resistances. This work demonstrates clearly the capability and potential advantages of IS as a tool for the complete characterization of TE materials. However, it is should be noted that this technique is only effective for TE materials with a moderate or large zT values. If $zT < 0.1$, the semicircle on the Nyquist plot cannot easily be observed.

IV. CONCLUSIONS

IS has been analyzed as a tool for the characterization of TE materials and devices. This work has led to the

development of suitable equivalent circuits that provide excellent fit to the impedance response of TE processes. Using the equivalent circuit, which consists of a pure resistance connected in series with two parallel-connected Warburg elements, several key TE parameters can be extracted from a relatively simple impedance measurement. This provides potentially an effective and rapid technique for characterization of TE properties.

The experimental study shows that, with the knowledge of the Seebeck coefficient, all key thermal parameters (including thermal diffusivity, thermal conductivity, and specific heat) of a TE element can be determined from the impedance spectrum. Furthermore, if a test is performed using a TE module, all the key TE properties (including the Seebeck coefficient, electrical resistivity, thermal conductivity, thermal diffusivity, specific heat, and zT) of the TE materials can be estimated. The results demonstrate clearly the capability of the impedance method as an effective tool for the evaluation of TE devices and the feasibility for a complete characterization of TE materials.

ACKNOWLEDGMENTS

[1] F. Fabregat-Santiago, G. Garcia-Belmonte, I. Mora-Sero, and J. Bisquert, Phys. Chem. Chem. Phys. **13**, 9083 (2011).

[2] I. Mora-Sero, G. Garcia-Belmonte, P. P. Boix, M. A. Vazquez, and J. Bisquert, Energy Environ. Sci. **2**, 678 (2009).

[3] X. Z. Yuan, H. J. Wang, J. C. Sun, and J. J. Zhang, Int. J. Hydrogen Energy **32**, 4365 (2007).

[4] R. Kotz, M. Hahn, and R. Gallay, J. Power Sources **154**, 550 (2006).

[5] G. W. Walter, Corrosion Sci. **26**, 681 (1986).

[6] J. Martin, T. Tritt, and C. Uher, J. Appl. Phys. **108**, 121101 (2010).

[7] T. M. Tritt and V. M. Browning, *Recent Trends in Thermoelectric Materials Research I* (2001), Vol. 69, p. 25.

[8] A. D. Downey, T. P. Hogan, and B. Cook, Rev. Sci. Instrum. **78**, 93904 (2007).

[9] A. De Marchi and V. Giaretto, Rev. Sci. Instrum. **82**, 034901 (2011).

[10] A. De Marchi and V. Giaretto, Rev. Sci. Instrum. **82**, 104904 (2011).

[11] E. Hatzikraniotis, K. T. Zorbas, I. Samaras, T. Kyratsi, and K. M. Paraskevopoulos, J. Electron. Mater. **39**, 2112 (2010).

[12] D. E. Wesolowski, R. S. Goeke, A. M. Morales, S. H. Goods, P. A. Sharma, M. P. Saavedra, K. R. Reyes-Gil, W. C. G. Neel, N. Y. C. Yang, and C. A. Apblett, J. Mater. Res. **27**, 1149 (2012).

[13] M. Lazard, C. Goupil, G. Fraisse, and H. Scherrer, Proc. Inst. Mech. Eng., Part A: J. Power Energy **226**, 277 (2012).

[14] J. Pailhes, C. Pradere, J. L. Battaglia, J. Toutain, A. Kusiak, A. W. Aregba, and J. C. Batsale, Int. J. Therm. Sci. **53**, 49 (2012).

[15] J. García-Cañadas and G. Min, J. Electron. Mater. **43**, 2411 (2014).

[16] J. R. Macdonald, *Impedance Spectroscopy* (Wiley, 1987).

[17] J. R. Macdonald, J. Phys. Chem. C **117**, 23433 (2013).

[18] H. Wang, W. D. Porter, H. Bottner, J. Konig, L. D. Chen, S. Q. Bai, T. M. Tritt, A. Mayolet, J. Senawiratne, C. Smith, F. Harris, P. Gilbert, J. Sharp, J. Lo, H. Kleinke, and L. Kiss, J. Electron. Mater. **42**, 1073 (2013).

[19] F. Casalegno, A. De Marchi, and V. Giaretto, Rev. Sci. Instrum. **84**, 024901 (2013).